



Effect of distilled water at high temperature on ductility and low-cycle fatigue of steel 10MgNi2MoV

Abshenov Kh.A.¹ , Arapov B.R.¹ , Seitkazenova K.K.¹ , Pecherskiy V.N.¹ ,
Zailybek B.B.*¹ , Mishra B.M.² , Kedelbayev B.Sh.¹ , Takibayeva G.A.¹ 

¹ M. Auezov South Kazakhstan Research University, Kazakhstan,

² Worcester Polytechnic Institute, USA

Abstract. The results of experimental tests of 10MgNi2MoV steel samples for low-cycle fatigue at various deformation rates in air and in distilled water at a temperature of 280 °C in a rigid loading mode with a symmetrical change in the range of elastic-plastic deformations are presented.

Since it is technically difficult to create real operating conditions for the material of a nuclear reactor vessel and a steam generator in laboratory conditions, the authors of the article created testing equipment. The results of experimental tests have shown that high-temperature distilled water significantly reduces the durability of steel than air.

The composition of the water has a great influence; it has been found that neutral water is less damaging than water with high acidity. Distilled water of these parameters, along with a decrease in the cyclic strength of steel, significantly affects its plastic properties. It has been established that during low-cycle deformation in high-temperature water, the plasticity of steel is significantly affected by the rate of elastic-plastic deformation of the material. Plasticity decreases at a certain critical range of deformation rates.

A mathematical model of the change in the ductility of steel in high-temperature water from the rate of deformation of the material is presented.

It has been established that the operating mode of the equipment must be organized so that the deformation rates of the bearing elements are far from the critical deformation rates obtained experimentally.

Keywords: steel ductility, deformation rate, structural steels, material durability, structural reliability, corrosion-mechanical damage, high-temperature corrosion, load-bearing elements, service strength, materials of critical structures, elements of power installations

Please cite this article as: Abshenov Kh.A., Arapov B.R., Seitkazenova K.K., Pecherskiy V.N., Zailybek B.B., Mishra B.M., Kedelbayev B.Sh., Takibayeva G.A. Effect of distilled water at high temperature on ductility and low-cycle fatigue of steel 10MgNi2MoV. *Construction Materials and Products*. 2026. 9 (2). 1. DOI: 10.58224/2618-7183-2026-9-2-1

*Corresponding author E-mail: bakdaulet.zhailybek@mail.ru

1. INTRODUCTION

For the safe operation of nuclear reactors, it is important to know the factors limiting the service life of both the reactor and the elements of the NPP production lines. These include neutron radiation, temperature, and corrosive environment, static and cyclic loads [1, 2, 3]. Each of these factors can lead to degradation of material properties and accumulation of damage, which at a certain stage of operation can cause the occurrence and development of defects, as well as destruction in certain areas of the reactor. The materials used must have the necessary strength characteristics, ductility and viscosity [4, 5].

To protect the housing from corrosion that may occur upon contact with the coolant, the inner surface is coated with stainless steel or other corrosion-resistant alloys [6, 7]. Austenitic stainless steel grade 08Cr18Ni10Ti or AISI 304/316 is usually used. This material is resistant to corrosion under high temperature and pressure conditions typical of an aquatic environment [8, 9]. The outer contour of the reactor and its components are made of low-alloy steel that is resistant to corrosion [10, 11].

High-temperature and high-pressure distilled water, used as a heat carrier (coolant) in the primary circuit of a water-water reactor (WWR) of a nuclear thermal power plant, reduces the strength and plastic properties of the vessel steel during long-term operation [12, 13].

Studies have established a decrease in the plastic properties of 10MgNi2MoV steel under the influence of high-temperature water at various deformation rates of the samples in experimental tests [14, 15].

Currently, regulatory engineering calculations of the strength and durability of nuclear reactor housings and other technological equipment are performed using guaranteed strength and ductility properties of reactor materials, steam generators, pipelines and other supporting elements of a nuclear power plant [16, 17].

Material destruction processes in high-temperature water environments involve complex corrosion-mechanical and electrochemical processes, which are influenced by the water's purity and composition, temperature, pressure, and flow conditions [18, 19]. Despite the need to establish the degradation patterns of materials under these conditions, there are currently no specific experimental studies on the kinetics of metal corrosion and the change of mechanical properties, particularly the study of the influence of boric acid in the primary circuit water of a nuclear power plant [20, 21]. This situation represents a significant knowledge gap that requires targeted research efforts.

Engineering strength calculations for highly loaded structural elements of power units must be carried out with the following scientifically substantiated and reliable data:

- the nature of the equipment's operational load, its operating temperature ranges, environmental conditions, and the guaranteed physical and mechanical properties of the structural materials;
- the reliably determined stress-strain state of the structural elements at the locations of structural stress concentrators;
- standardized calculation models that allow for the calculation of the service life of the designed equipment and the residual service life of existing equipment based on the information provided in the previous two points [22, 23, 24]. At the first stage of strength engineering calculations based on allowable stresses, the main dimensions of the structure are determined. At the second stage, a verification calculation is carried out, based on which the geometric shape and dimensions of structural elements, the allowable number of loading cycles, and the service life are specified more precisely [25, 26, 33].

During the verification calculation, in the computational models [27, 28], stresses are calculated assuming elastic behavior of the material; including cases where the stresses obtained from calculations exceed the material yield strength. In the calculation equations relating conventionally elastic allowable stresses to the number of loading cycles, alongside strength characteristics, the material plasticity characteristics are of significant importance [29, 30]. Therefore, it is essential to have actual values of the plastic properties of pressure vessel steels experimentally determined under various loading conditions with the simultaneous action of a corrosive environment [31, 32].

2. METHODS AND MATERIALS

In this study, heat-resistant alloy steel 10MgNi2MoV was used, the chemical composition and mechanical properties of which are given in Tables 1 and 2.

Table 1. Chemical composition of 10MgNi2MoV steel (mass fraction, %).

C	Mn	Si	Ni	S	P	Cr	Mo	V	Cu
0.08–0.12	0.8–1.1	0.17–0.37	1.8–2.3	to 0.02	to 0.02	to 0.3	0.4–0.7	0.03–0.07	to 0.3

Table 2. Mechanical properties of 10MgNi2MoV steel at a temperature of 20 °C.

tensile strength σ_t , MPa	yield strength, σ_{ys} , MPa	elongation δ , %	reduction in area ψ , %	KCU, K j/m ²
540-700	340-590	16	55	390

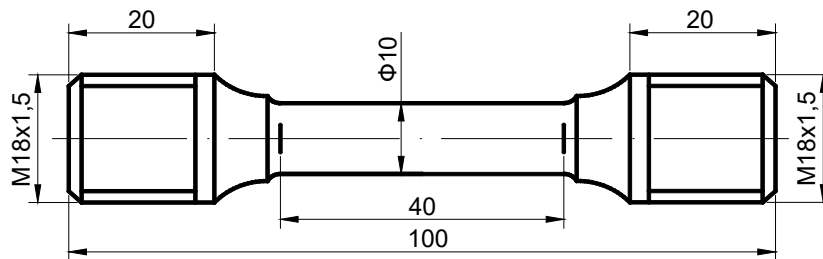


Fig. 1. Shapes and geometric dimensions of the test sample.

Cylindrical samples with a diameter of 10 mm and a working length of 40 mm, shown in Figure 1, were tested.

The tests were carried out at nine levels of the elastic–plastic strain range of the sample, listed in Table 1, under symmetric cyclic loading.

For axial tensile and low-cycle fatigue tests, a test chamber shown in Fig. 2 was used. The chamber consists of a thick-walled cylindrical vessel, a cover, and a loading piston, all fabricated from 08Cr18Ni10Ti stainless steel. High pressure of the distilled water in the chamber was generated by a plunger pump, while water heating was provided by an electric heater located around the cylindrical part of the chamber on its outer surface. The deformation of the test sample was measured using a mechanical extensometer mounted on the surface of the sample positioned inside the chamber, the measuring blades of which are kinematically connected by tractions of ferromagnetic cores of an inductive transducer.

Table 3. Elastic–plastic strain range.

Range of the deformation, $\Delta\varepsilon$, %	0.5	0.6	0.7	0.8	1.0	1.2	1.4	1.6	1.7
---	-----	-----	-----	-----	-----	-----	-----	-----	-----

To comparatively assess the effect of distilled water on plasticity and low-cycle strength, the tests were also carried out in air at the corresponding temperature. Standard plasticity characteristics were determined after the destruction of the sample using the following formulas:

Residual elongation

$$\delta = \frac{l - l_0}{l_0}$$

Coefficient of narrowing of the cross-sectional area

$$\psi = \frac{A_0 - A_1}{A_0}$$

where: $l_0=20$ mm is the initial length, the base for measuring deformations;

l_1 is the length of the measurement base after the destruction of the sample;

A_0 is the cross-sectional area of the sample before destruction;

A_1 is the cross-sectional area of the sample at the site of the "neck" formation.

The tensile rate of the sample (moving the active grip of the testing machine) was calculated as a function of the specified strain rate of the sample according to the following formula:

$$V = 60 \cdot l_0 \cdot \dot{\epsilon} \quad (1)$$

where: V – the displacement rate of the active grip of the testing machine, [mm/min]; $\dot{\epsilon}$ – the deformation rate of the working part of the test sample, [s^{-1}].

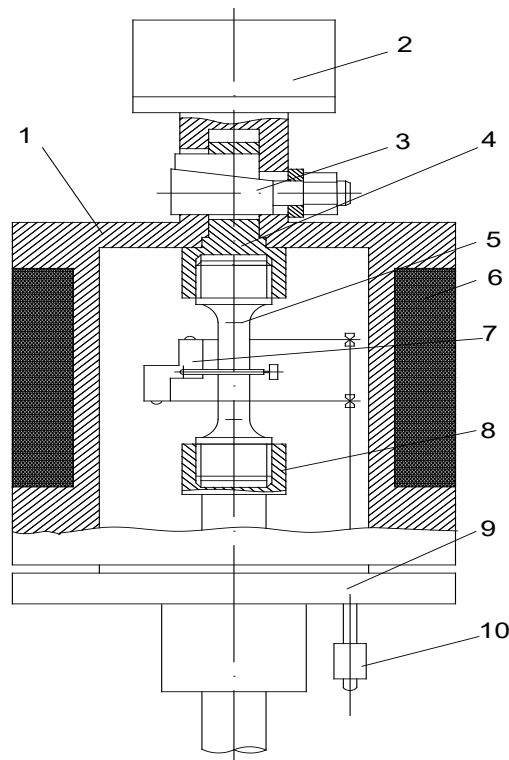


Fig. 2. Test procedure using the experimental chamber: 1 – chamber body, 2 – fixed grip, 3 – wedges, 4 – shank, 5 – test sample, 6 – electric heater, 7 – mechanical extensometer body, 8 – active grip, 9 – chamber cover, 10 – inductive displacement sensor.

Test Procedure Using the Chamber Shown in Fig. 2. With the chamber cover (9) removed together with the active grip (8), the test sample (5) is screwed by one threaded end into the socket located at the end face of the active grip (8). A mechanical extensometer (7) is then installed on the gauge section of the sample over a measuring base of 20 mm; its measuring rods are connected to the ferromagnetic tips of the inductive displacement sensor (10). A shank (4) is screwed onto the other

end of the sample. The assembled active grip with the test sample, together with the chamber cover, is inserted into the chamber so that the shank (4) engages a special socket at the bottom of the chamber body (1) equipped with a wedge mechanism (3). The wedge mechanism ensures reliable fixation of the shank and the sample within the chamber body while simultaneously providing chamber sealing. The chamber cover (9) is fastened to the body using bolts through a sealing gasket made of stainless steel with a rhombic cross-sectional shape, thereby ensuring tightness of the chamber working space. The fully assembled chamber is connected by its fixed grip (2) to the fixed crosshead of the testing machine, while the force rod is connected to the active grip of the machine. After filling the chamber with distilled water and increasing the pressure to the required level, the electric heater (6) is switched on. Once the specified temperature is reached, the testing machine is activated according to the prescribed test regime for the sample.

In the works of the authors [12, 13, 14], K_ψ and K_δ plasticity characteristic coefficients are introduced that show the reduction in metal plasticity in a corrosive environment compared to its plasticity in air:

$K_\psi = \frac{\psi_{ce}}{\psi_{air}}$ - a coefficient indicating the degree of reduction in the residual relative decrease of the cross-sectional area of the test sample;

$K_\delta = \frac{\delta_{ce}}{\delta_{air}}$ - a coefficient indicating the degree of reduction in the residual relative elongation of the test sample.

where: ψ_{ce} , ψ_{air} and δ_{ce} , δ_{air} - the relative reduction of the cross-sectional area and the relative elongation in a corrosive environment and in air, respectively.

When conducting low-cycle fatigue tests, the frequency of cyclic loading that ensured the specified deformation rates was determined using the following calculations:

The displacement of the active grip of the machine during one half-cycle of strain-controlled low-cycle loading is equal to

$$\Delta \varepsilon = \frac{\Delta l}{l_0} \cdot 100\% = \frac{\Delta l}{20} \cdot 100\%, \quad \Delta l = \frac{20 \cdot \Delta \varepsilon}{100} = 0.2 \cdot \Delta \varepsilon \text{ mm} \quad (2)$$

Then, the total displacement of the active grip during one symmetric cycle is equal to

$$l = 2 \cdot \Delta l = 2 \cdot 0.2 \cdot \Delta \varepsilon = 0.4 \cdot \Delta \varepsilon \text{ mm} \quad (3)$$

The relative strain rate of the sample over a 20 mm gauge length is equal to $\dot{\varepsilon} = \frac{\Delta l}{20 \cdot 60} \text{ s}^{-1}$.

The time required for one loading cycle is equal to $t = \frac{l}{\dot{\varepsilon}}$. (4)

$$t = \frac{l}{\dot{\varepsilon}} = \frac{0.4 \cdot \Delta \varepsilon}{\dot{\varepsilon}} = \frac{0.4 \cdot \Delta \varepsilon}{\dot{\varepsilon} \cdot 60} \text{ min} = 0.00667 \cdot \frac{\Delta \varepsilon}{\dot{\varepsilon}} \text{ min.}$$

Then the frequency of symmetric strain-controlled low-cycle loading is equal to

$$f = \frac{1}{t} = \frac{\dot{\varepsilon}}{0.00667 \cdot \Delta \varepsilon} = 150 \frac{\dot{\varepsilon}}{\Delta \varepsilon} \text{ cycles/min} \quad (5)$$

In accordance with the capabilities of the gearbox of the testing machine, the tests were conducted at the following sample deformation rates, as shown in Table 4.

Table 4. Sample deformation rates and frequencies of cyclic strain-controlled low-cycle loading corresponding to the strain range $\Delta\varepsilon=0,5\%$.

Deformation rate, $\dot{\varepsilon}$, s^{-1}	$1 \cdot 10^{-3}$	$1.15 \cdot 10^{-4}$	$1.15 \cdot 10^{-5}$	$1.4 \cdot 10^{-5}$	$1.6 \cdot 10^{-5}$	$1.25 \cdot 10^{-6}$	$1.8 \cdot 10^{-6}$
Cyclic loading frequency, cycles/min	0.3	0.0345	0.00345	0.0042	0.0048	0.0048	0.0048

The cyclic loading frequency for each elastic–plastic strain range corresponding to a given deformation rate is calculated using the formulas (4) and (5).

Low cycle fatigue tests. The samples were tested under symmetric cyclic deformation at a prescribed frequency and cyclic strain ranges from $\Delta\varepsilon=0.5\%$ to 1.7% with an increment of 0.2% at each test step. The frequency of low-cycle loading, depending on the elastic–plastic strain range and the specified deformation rate, varied from 0.0024 cycles/min to 0.3 cycles/min. The tests were performed both in air and in distilled water at a temperature of 280 °C. The strain range of the test sample was set based on the displacement of the loading rod using a previously established calibration curve.

The diagram of cyclic elastoplastic deformation during the tests was periodically recorded on a two-axis recorder of the PDP-002 brand.

A universal electromechanical testing machine UME-10TM equipped with a heating system and automatic maintenance of the specified water temperature in the chamber was used for the experiments[31, 32].

3. RESULTS AND DISCUSSION

During the tests, experimental data was obtained and is presented in Figure 3. As can be seen from the results, distilled water at a temperature of 280 °C significantly reduces the cyclic strength of 10MgNi2MoV steel.

The experimental results also indicate that the effect of water depends on its acidity. As shown in Fig. 3, neutral water with a pH value of 7 (neutral environment) is less damaging compared to acidic water with a pH of 4.

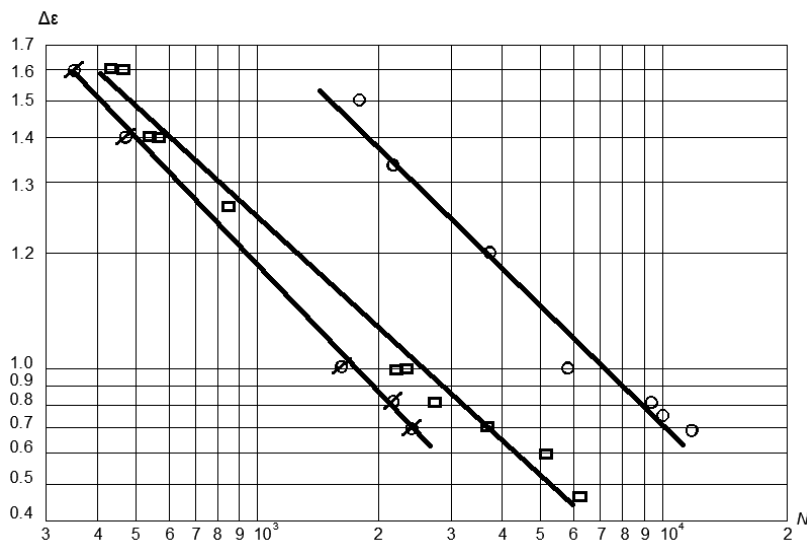


Fig. 3. Low-cycle fatigue curves of 10MgNi2MoV steel samples obtained from tests in air and in distilled water with different acidity at a temperature of 280 °C.

As can be seen from Fig. 3, the reduction in durability in neutral distilled water compared to air amounts to 60% at an elastic–plastic strain range of $\Delta\varepsilon=1.4\%$, and to 62% at a range of $\Delta\varepsilon=0.7\%$, which indicates an identical degree of influence (within the limits of experimental error) of neutral distilled water with pH = 7 at the investigated elastic–plastic strain range levels.

The reduction in fatigue life in acidic distilled water with pH = 4 amounts to 72% at an elastic–plastic strain range of $\Delta\varepsilon=1.4\%$, and to 76% at a strain range of $\Delta\varepsilon=0.7\%$. These results indicate that the effect of high-temperature water on the metal slightly increases with a decrease in the cyclic strain range level.

After samples fracture, the standard plasticity characteristics ψ_{ce} , ψ_{air} and δ_{ce} , δ_{air} , were determined. Based on the results of examinations of samples tested both in air and in distilled water, the plasticity reduction indices were calculated in the form of coefficients K_ψ and K_δ .

The investigation of sample plasticity, determined as K_ψ and K_δ , after fracture showed that the deformation rate has a significant effect on plasticity indicators in the deformation rate range from 10^{-5} s⁻¹ to 10^{-6} s⁻¹.

Figure 4 presents the patterns of change in the plasticity of 10MgNi2MoV steel samples during low-cycle fatigue testing under strain-controlled loading in water at a temperature of 280 °C, as a function of the deformation rate of the steel sample.

As can be seen from the graphs (Fig. 4), there exists a deformation rate region at which the maximum reduction in steel plasticity is observed. This region can be characterized as the critical deformation rate of the material.

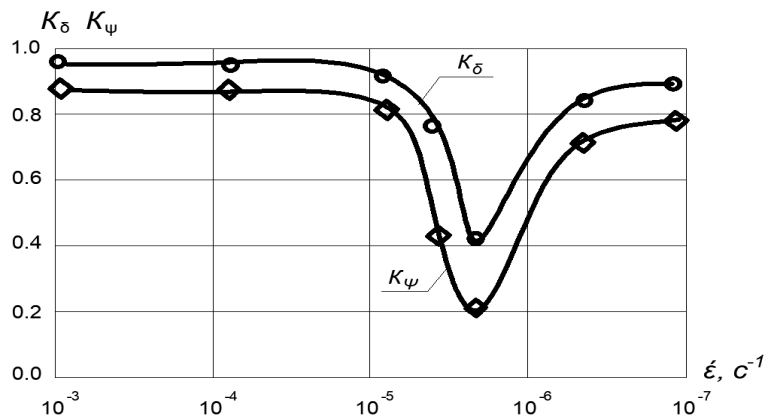


Fig. 4. Patterns of change in the coefficients of plasticity characteristics of 10MgNi2MoV steel in distilled water depending on the strain rate $\dot{\varepsilon}$ at a temperature of 280°C.

Metallographic examinations of the surface and longitudinal sections of samples after completion of testing in distilled water have established that the primary cause of steel sample failure in high-temperature water is the formation of numerous corrosion cracks oriented perpendicular to the direction of tensile stresses (Fig. 5). The initiation and propagation of these corrosion cracks within the metal begin with the cracking of the surface oxide layer composed of brittle magnetite that forms on the sample surface in high-temperature water.

Studies reported in Refs. [15, 16] have shown that the embrittlement and cracking of metal exposed to a corrosive environment are caused by tensile stresses, which is in good agreement with the data obtained in the present work.

Cracking of the surface magnetite layer formed on the steel surface in high-temperature water, which normally protects the metal from corrosive damage, leads to the dissolution of bare metal at the sites where the magnetite film is damaged. As a result, loosening of the near-surface metal layer occurs. The initiation and propagation of surface corrosion cracks in the metal cause stress

concentration at the crack tips, which leads to embrittlement and accelerated failure of the material. The deformation rate also has a significant effect on the embrittlement process. It has been established that intense metal embrittlement in high-temperature water occurs within the so-called “critical” deformation-rate range of steel, where the lowest plasticity characteristics are observed.

The results of experimental tensile tests at low deformation rates and low-cycle fatigue tests of high-strength 10MgNi2MoV steel samples under the action of high-temperature distilled water have shown that the plastic properties of the metal strongly depend on the deformation rate. The most sensitive parameter in this case is the reduction of area coefficient of the test samples (Fig. 4). In the range of so-called “critical” deformation rates, as demonstrated by our studies, the reduction of area coefficient ψ decreased to its minimum value.

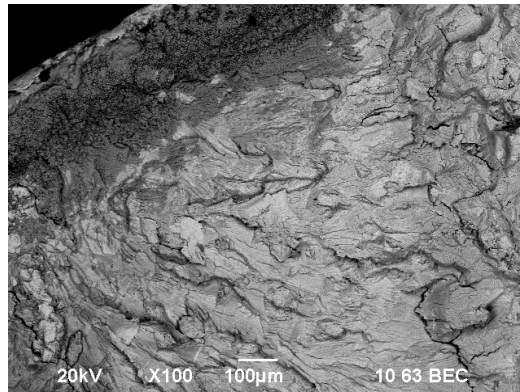


Fig. 5. Corrosion cracking cracks of 10MgNi2MoV steel in chloride-containing water at 80°C in the cross-section of the sample after rupture.

Based on the experimental data obtained on cyclic corrosion strength and the corresponding reductions in material plasticity, it can be stated that, within the range of critical deformation rates, an important role in the accumulation of corrosion–fatigue damage is played by local failures caused by anodic dissolution of the metal at the tips of the formed micro cracks, leading to metal embrittlement. Therefore, the development of a methodology for determining the actual deformation rates of load-bearing structural elements during operation is of substantial importance, as these rates correspond to different operating regimes of the installation and to the plasticity characteristics of the steel under these regimes.

For this purpose, to mathematically describe the dependence of the plasticity indicator of the load-bearing metal on the deformation rate using experimental data, we have proposed a model of the following form:

$$\psi_{ce}^T = \psi_{st}^T \left[1 - \alpha \lg \frac{\dot{\epsilon}_{st}}{\dot{\epsilon}} - \beta \frac{1}{e^{\left(\frac{\dot{\epsilon}_{cr} \dot{\epsilon}}{e^{\gamma \dot{\epsilon}_{cr}}} \right)}} \right] \quad (6)$$

where ψ_{ce}^T is the plasticity indicator of the steel corresponding to the operational deformation rate and the ambient temperature $\dot{\epsilon}$;

ψ_{st}^T – the plasticity characteristic of the steel obtained from standard tests in air at the same temperature;

$\dot{\epsilon}_{st}$ – the deformation rate under standard testing methods;

$\dot{\epsilon}_{cr}$ – the critical deformation rate at which the maximum reduction in steel plasticity is observed;

α, β, γ – coefficients determined from low-strain-rate static tensile tests in a corrosive environment based on the best fit to the experimental data.

The second term of the multiplier in equation (6), given in parentheses, determines the degree of monotonic variation of steel plasticity, which depends on the duration of environmental exposure to the metal and characterizes a gradual decrease in plasticity with decreasing deformation rate. The monotonic decrease in steel plasticity over time occurs as a result of the simultaneous action of adsorption-induced wedge effects, hydrogen embrittlement, and anodic dissolution. The sharp reduction in steel plasticity in the region of critical deformation rates is associated with the predominance of one of these factors. Under high-temperature water conditions, when a thin protective magnetite film is formed on the metal surface, the pronounced decrease in metal plasticity is caused by the predominance of anodic dissolution of the steel.

In the region of critical metal deformation rates, the anodic dissolution of the metal increases in its local areas. This is promoted by a favorable combination of the metal deformation rate, which is associated with the intensity of destruction of the surface protective magnetite layers, and the rate of anodic dissolution at the sites where the protective magnetite film has been damaged.

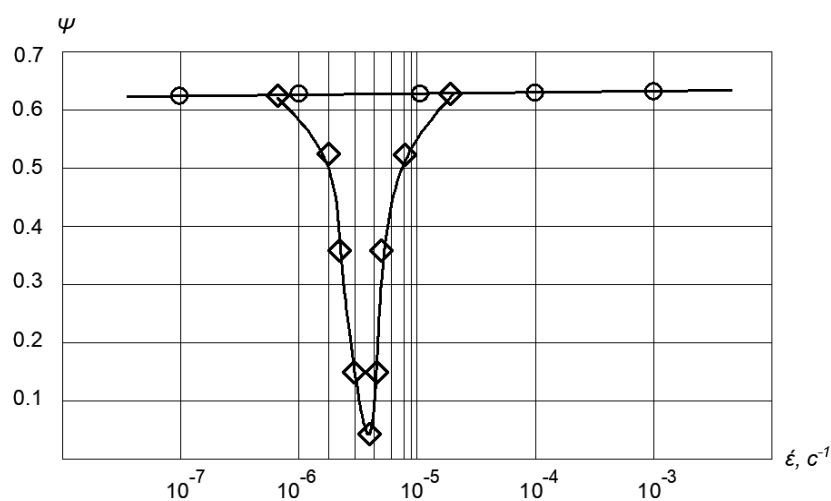
When the deformation rate is equal to the critical value, passivation of the surface (i.e., formation of a protective film) apparently does not occur at local zones where the magnetite film is destroyed and anodic dissolution is intensified, which leads to the intensive development of corrosion cracking and, consequently, to steel embrittlement.

If the deformation rate of the steel exceeds its critical value, the mechanical deformation processes outpace the chemical processes, and anodic dissolution cannot exert a significant effect on the plastic properties of the steel. In this case, the deformation process approaches that of a short-term standard tensile test in a corrosive environment, which leads many researchers to conclude that the corrosive environment does not have a significant effect on steel plasticity.

When the deformation rate of the sample is lower than the critical rate, the anodic dissolution process outpaces the deformation process, resulting in the formation of a dense protective magnetite film that is no longer destroyed due to the low deformation rate. The maximum manifestation of anodic dissolution is observed at a deformation rate equal to the critical one; in all cases, deviations from this value in either direction lead to a reduction in anodic metal dissolution and, accordingly, to a decrease in the cracking process.

The influence of the critical deformation rate on metal plasticity in equation (6) is taken into account by the third term in the parentheses. The monotonic decrease in plasticity, mainly associated with the hydrogen embrittlement factor, can be considered uniform and independent of the deformation rate of the metal, since these processes reach their equilibrium state over a prolonged

period under steady conditions. Then, the coefficient α in equation (6) can be determined without taking the third term into account, as shown in Fig. 6.



● – data obtained in air; ◆ – data obtained in distilled water;

Fig. 6. Patterns of change in plasticity of 10MgNi2MoV steel depending on the rate of deformation.

From the experimental results, initial and final plasticity ψ^T values are obtained, corresponding to the highest and the lowest deformation rates of the sample in the given test series. As can be seen from Figure 6, all intermediate values of ψ^T , except for those corresponding to the critical deformation rate, fall approximately on a straight line in semilogarithmic coordinates. Therefore, the experimental data values are converted into relative dimensionless quantities, i.e., $\psi^T \%/100$, and then:

At $\dot{\varepsilon}=\dot{\varepsilon}_{initial}$, the plasticity is equal to $\psi^T=\psi_{initial}^T$; similarly, At $\dot{\varepsilon}=\dot{\varepsilon}_{ultimate}$, the plasticity is equal to $\psi^T=\psi_{ultimate}^T$, and on the basis of formula (6) we obtain:

$$\begin{aligned} \psi_{initial}^T \psi_{ultimate}^T &= \alpha \left(\lg \frac{\dot{\varepsilon}_{st}}{\dot{\varepsilon}_{ultimate}} - \lg \frac{\dot{\varepsilon}_{st}}{\dot{\varepsilon}_{initial}} \right) \\ \alpha &= \frac{\psi_{initial}^T \psi_{ultimate}^T}{\lg \left(\frac{\dot{\varepsilon}_{initial}}{\dot{\varepsilon}_{ultimate}} \right)} \end{aligned} \quad (7)$$

Since a sharp intensification of local anodic dissolution (metal embrittlement) in the region of critical deformation rates is superimposed on the monotonic process of plasticity reduction, the coefficient β is determined assuming that

$$\dot{\varepsilon}=\dot{\varepsilon}_{cr} \quad \text{to} \quad \psi^T=\psi_{cr}^T$$

from (6) we obtain

$$\begin{aligned} \psi_{cr}^T &= \psi_{st}^T \left[1 - \alpha \lg \frac{\dot{\varepsilon}_{st}}{\dot{\varepsilon}_{cr}} - \beta \frac{1}{e^{\gamma \left(\frac{\dot{\varepsilon}_{cr}}{\dot{\varepsilon}_{st}} \right)^2}} \right] \quad \text{where} \\ \beta &= 1 - \alpha \lg \frac{\dot{\varepsilon}_{st}}{\dot{\varepsilon}_{cr}} - \frac{\psi_{cr}^T}{\psi_{st}^T} \end{aligned} \quad (8)$$

The coefficient γ is determined from equation (6) by processing the experimental data on deformation rates in the critical regions using the least squares method.

Based on the experimental data obtained for 10MgNi2MoV steel in distilled water, the following values of these coefficients were determined:

$$\alpha=0.013; \quad \beta=0.89; \quad \gamma=0.45$$

Depending on the operational load of the equipment, its load-bearing elements, for example, the housing of a steam generator of a nuclear power plant made of steel 10MgNi2MoV, can experience deformation at different rates. Therefore, using equation (6), it is possible to calculate the current value of the plasticity characteristic of a structural element that is simultaneously subjected to mechanical deformation and a corrosive environment in the form of high-temperature water.

Thus, based on the proposed model (6), which describes the patterns of changes in the plasticity of a material from the rate of deformation, the values of plasticity in a high-temperature water environment are established at various rates of cyclic deformation, under low-cycle loading with low deformation rates. Based on the experimentally obtained data shown in Figure 5, it is possible to recommend a loading mode for the load-bearing elements of the equipment, in which the deformation rates do not coincide with the critical speeds.

When the daily power output of the reactor changes, the load-bearing elements may experience deformation at different rates.

When the power output of the reactor increases, the internal pressure in the steam generator gradually increases, which leads to an increase in the rate of deformation of the steam generator casing. When the water pressure in the steam generator decreases, the opposite process occurs, leading to a decrease in the rate of deformation of the casing.

Thus, the material of the housing will be in a cyclically loaded state during the operation of the steam generator. Under these conditions, the rates of deformation of the material will change according to some arbitrary laws in the areas of stress concentration of the loaded element, reaching their maximum and minimum values and repeatedly passing through the critical rate of deformation.

Therefore, in order to calculate the strength and determine the durability of a structural element under the influence of corrosion-mechanical low-cycle loading, it is necessary to properly establish the patterns of change in the available plasticity of the material under operational conditions, in order to use them in regulatory calculation models based on deformation criteria for cyclic strength.

Deformation rates close to critical values can be determined based on the equation of the mechanical state and the stress-strain state at the points of stress concentration.

To do this, we use equation (6), which allows us to calculate the current value of the plasticity characteristic of a structural element made of given steel that is simultaneously subjected to mechanical stress and a corrosive environment.

Since, during laboratory testing, the nominal deformation rate of a sample can be prescribed, the constancy of the заданная deformation rate is evidently valid for the sample material only up to the moment when micro cracks begin to form on its surface. The appearance of micro cracks on the surface of the test sample leads to localization of deformation at the crack tip, where the metal deformation rate must be higher than the prescribed nominal deformation rate.

Examination of sample surfaces after fracture and of their longitudinal sections showed that, in the region of critical nominal deformation rates, the formation of numerous cracks oriented perpendicular to the direction of tensile stresses was observed. This indicates that under these conditions the reduction in material plasticity occurs due to the formation of surface micro cracks. Subsequently, the preferential development of one of these micro cracks leads to the formation of a main crack, which ultimately results in failure of the structural element.

The formation of surface macro cracks significantly reduces the difference between the nominal deformation rate of the test sample and the local deformation rate at the tips of corrosion cracks.

To assess the degree of difference between these rates, the relationship between the nominal deformation of the sample and the deformation in stress concentration zones at the crack tip is considered. The stress and strain concentration factors in the elastic-plastic region are related to the elastic stress concentration factor α_σ by the following relationship [17, 18, 19].

$$\frac{K_\sigma K_\varepsilon}{\alpha_\sigma^2} = 1 \tag{9}$$

According to experimental data and calculations by Makhutov N., Serensen S., and others [18,19,20,21], the unity on the right-hand side of equation (9) is replaced by the following function.

$$F[\alpha_\sigma, \bar{\sigma}_n, f(\bar{\sigma}_n, \bar{\varepsilon}_n)] = \frac{1}{(\alpha_\sigma \bar{\sigma}_n)^{n(1-\beta)} [1 - (\bar{\sigma}_n / \alpha_\sigma)]} \tag{10}$$

Then, taking (10) into account, equation (9) takes the following form

$$\frac{K_\sigma K_\varepsilon}{\alpha_\sigma^2} = \frac{1}{(\alpha_\sigma \bar{\sigma}_n)^{n(1-\beta)} [1 - (\bar{\sigma}_n / \alpha_\sigma)]} \tag{11}$$

where K_σ and K_ε – the stress and strain concentration factors, respectively;

α_σ – the theoretical stress concentration factor in the elastic region;

n – a constant determined from calculations or experiments for the given conditions α_σ and $\bar{\sigma}_n$;

ν – the exponent in the power-law approximation of the deformation diagram.

In relative coordinates, where $\bar{\sigma}_n = \frac{\sigma_n}{\sigma_c}$ and $\bar{\epsilon}_n = \frac{\epsilon_n}{\epsilon_c}$ are the nominal stresses and nominal strains, these quantities are related by the following relationships:

$$\begin{aligned} \bar{\sigma}_n &= \bar{\epsilon}_n, \text{ with } \bar{\sigma}_n \leq 1 \\ \bar{\sigma}_n &= \bar{\epsilon}_n^\nu, \text{ with } \bar{\sigma}_n > 1, \text{ a power approximation.} \end{aligned} \quad (12)$$

Similarly, for stress concentration zones (crack tip), the following can be written:

$$\begin{aligned} \bar{\sigma}_{maxk} &= \bar{\epsilon}_{maxk}, \text{ with } \bar{\sigma}_{maxk} \leq 1 \\ \bar{\sigma}_{maxk} &= (\bar{\epsilon}_{maxk})^\nu, \text{ with } \bar{\sigma}_{maxk} > 1, \end{aligned} \quad (13)$$

Since $\bar{\sigma}_{maxk} = K_\sigma \cdot \bar{\sigma}_n$ and $\bar{\epsilon}_{maxk} = K_\epsilon \cdot \bar{\epsilon}_n$, on the basis of (10), we obtain

$$K_\sigma = \frac{K_\epsilon^\nu \cdot \bar{\epsilon}_n^\nu}{\bar{\sigma}_n} \quad (14)$$

Then, taking (11) into account, from (8):

$$K_\epsilon = \frac{\alpha_\sigma^{\frac{2}{(1+\nu)}} \cdot \bar{\sigma}_n^{\frac{(1-\nu)}{(1+\nu)}}}{(\alpha_\sigma \cdot \bar{\sigma}_n)^{\nu(1-\nu)} [1 - (\bar{\sigma}_n \alpha_\sigma^{-1})]^\nu / (1+\nu)}, \text{ with } \bar{\sigma}_n \leq 1 \quad (15)$$

$$K_\epsilon = \frac{\bar{\sigma}_n^{\frac{(1-\nu)}{(1+\nu)}}}{(\alpha_\sigma \cdot \bar{\sigma}_n)^{\nu(1-\nu)} [1 - (\bar{\sigma}_n \alpha_\sigma^{-1})]^\nu / (1+\nu)}, \text{ with } \bar{\sigma}_n > 1 \quad (16)$$

The maximum deformation at the crack tip $\bar{\epsilon}_{maxk}$ is related to the nominal deformation $\bar{\epsilon}_n$ through the strain concentration factor.

$$\bar{\epsilon}_{maxk} = K_\epsilon \cdot \bar{\epsilon}_n \quad (17)$$

According to (16), the theoretical stress concentration factor at the crack tip is determined by the formula

$$\begin{aligned} \alpha_\sigma &= \frac{1}{\bar{\sigma}_n} \cdot \frac{\bar{K}_1}{\sqrt{2\pi l}} - \text{for a plane stress state} \\ \alpha_\sigma &= \frac{\sqrt{1-2\mu}}{\bar{\sigma}_n} \cdot \frac{\bar{K}_1}{\sqrt{2\pi l}} - \text{for plane strain} \end{aligned} \quad (18)$$

Where \bar{K}_1 is the stress intensity factor, determined by the formula

$$\bar{K}_1 = \bar{\sigma}_n \sqrt{\pi l} f(\lambda) \quad (19)$$

where l is the crack length;

$f(\lambda)$ – a correction function depending on the crack depth and the shape and dimensions of the structural element;

r – the distance from the surface of the element to the crack tip in the direction of crack growth.

$$\bar{K}_I = \bar{\sigma}_n \sqrt{\pi r} f(\lambda) \quad (19)$$

Thus, it can be assumed that the deformation rate at the tip of a formed macro crack is higher than the nominal deformation rate by a value equal to the product of the nominal deformation rate and the strain concentration factor.

$$\dot{\varepsilon}_{crack} = \dot{\varepsilon}_n \cdot K_\varepsilon \quad (20)$$

The value of the deformation rate and, accordingly, the plasticity index at the crack tip will subsequently determine the crack growth rate and, accordingly, the material survivability at the crack growth stage.

4. CONCLUSIONS

1. High-temperature distilled water, which is the heat carrier circulating in the first loop of water-water (WW) nuclear reactors, significantly reduces the low-cycle fatigue strength of 10MgNi2MoV steel, which is used in the manufacturing of steam generator components for nuclear power plants.

2. The effect of the deformation rate of steel on its plastic characteristics has been experimentally established, and there is a certain range of deformation rates in which the plasticity of steel in high-temperature water decreases sharply.

3. This phenomenon has been taken into account in practice during the operation of power plants, which is an important factor in calculating the strength of load-bearing elements of the structures and in properly organizing the operating conditions of equipment, as well as in establishing the safest operating modes that ensure their durability.

4. It has been established that the composition of distilled water also affects the low-cycle corrosion-fatigue strength of the investigated steel. It is shown that the purer the water, the less pronounced is the negative influence of the environment on the metal.

5. Equipment and fixtures have been developed for testing steel and alloy samples in corrosive environments, allowing laboratory simulation of operating parameters such as temperature, pressure, and chemical composition of aqueous solutions. A testing methodology has been developed to obtain strength and plasticity characteristics of steels under conditions close to actual operating conditions.

6. A mathematical model (equation) is proposed that describes the dependence of the plasticity of a material interacting with high-temperature water on the rate of deformation, and the existence of a critical rate of deformation is established, where the plasticity of steel is significantly reduced.

7. Based on the analysis of the obtained experimental low-cycle fatigue curves and the investigation of longitudinal sections of fractured samples, recommendations have been developed for organizing equipment operating modes such that, under service loading, the deformation rates of the metal of load-bearing components of power installations in contact with high-temperature water do not coincide with the critical deformation rate of this metal in the corresponding environment.

5. ACKNOWLEDGEMENTS

The research was carried out at the Research Laboratory “Problems of Mechanical Engineering” with the financial support of the Science Committee of the Ministry of Science and Higher Education of the Republic of Kazakhstan. (Grant No. AP26199289)

REFERENCES

1. Vilensky O.Yu., Dushev S.A., Lapshin D.A., Lebedev D.A., Shimin D.A. Models of material deformation under dynamic loading applied to various structural elements. *Atomic Energy*. 2025. P. 231 – 235. DOI:<https://doi.org/10.1007/s10512-025-01250-8>
2. Kulakov G.V., Konovalov Yu. V., Savchenko A.M., Corrosion of E110 alloy fuel element cladding in nuclear icebreaker reactors and small nuclear power plants. *Atomic Energy*. 2025. P. 35 – 39. DOI:<https://doi.org/10.1007/s10512-025-01223-x>
3. Smirnova L.S., Korolev S.A. Critical factors of integrated approach to economics of small modular reactors. *Atomic Energy*. 2025. P. 1 – 11. DOI: <https://doi.org/10.1007/s10512-025-01171-6>
4. Ortner S. Review of requirements for structural materials and their selection for nuclear power plants. *Frontiers in Nuclear Engineering*. 2023. P. 1 – 5. DOI: <https://doi.org/10.3389/fnuen.2023.1253974>
5. Hamdan H., Alsit A. Al Tahhan A.B., Mughieda O., Mourad A.,H.I., Shehadeh M.A., Alkhedher M., Prediction methods of stress corrosion cracking under harsh environmental conditions. *Heliyon*. 2024. P. 1 – 13. DOI:<https://doi.org/10.1016/j.heliyon.2024.e25276>
6. Ehrnstén U., Andresen P.L., Que Z. A review of stress corrosion cracking of austenitic stainless steels in PWR primary water. *Journal of Nuclear Materials*. 2024. P. 1 – 7. DOI: <https://doi.org/10.1016/j.jnucmat.2023.154815>
7. Fan Y., Lu Y.H., Wang F., Hong C., Shoji T. Development of stress corrosion cracking testing method in high-temperature high-pressure water using small punch test. *Nuclear Engineering and Design*. 2025. P. 1 – 12. DOI: <https://doi.org/10.1016/j.nucengdes.2025.113830>
8. Kuang W., Ma X., Meng F., Han E.H. Recent progress in research on stress corrosion crack initiation of alloy 690 in PWR primary circuit. *Results in Materials*. 2025. P. 20. DOI: <https://doi.org/10.1016/j.revmat.2025.100109>
9. Volokitina A., Volokitina I., Gelmanova Z., Denissova A. Thermomechanical treatment influence on the copper wire microstructure evolution. *Theoretical and Applied Mechanics Letters*. 2026. P. 16. DOI:<https://doi.org/10.1016/j.taml.2025.100650>
10. Volokitina A., Volokitina I., Panin E. Martensitic Transformation in AISI-316 Austenitic Steel During Thermomechanical Processing. *Metallography Microstructure and Analysis*. 2022. P. 673 – 675. DOI:<https://doi.org/10.1007/s13632-022-00877-4>
11. Volokitina I., Kolesnikov A., Fediuk R., Klyuev S., Sabitov L., Volokitina A., Zhuniskaliyev T., Kelamanov B., Yessengaliyev D., Yerzhanov A., Kolesnikova O. Study of the Properties of Antifriction Rings under Severe Plastic Deformation. *Materials*. 2022. 15 (7). P. 2584.
12. Betova I., Bojinov M., Karastoyanov V. Corrosion mechanism of austenitic stainless steel in high-temperature high-pressure water studied by impedance spectroscopy. *Metals*. 2025. P. 11 – 16. DOI:<https://doi.org/10.3390/met15080875>
13. Tukur H., Yonghao L. Review on the behavior of 308L cladding material and corrosion in nuclear power plants. *International Journal of Electrochemical Science*. 2020. P. 1005 – 1021. DOI:<https://doi.org/10.20964/2020.01.67>
14. Zhangabay N., Sapargaliyeva B., Suleimenov U., Abshenov Kh., Utelbayeva A., Baibolov K., Fediuk R., Arinova D., Duissenbekov B., Seitkhanov A., Amran M. Analysis of Stress-Strain State for a Cylindrical Tank Wall Defected Zone. *Materials*. 2022. P. 5732. DOI:<https://doi.org/10.3390/ma15165732>
15. Tursunkululy T., Zhangabay N., Suleimenov U., Abshenov Kh., Utelbayeva A., Moldagaliyev A., Turashova Zh., Karshyga G., Kozlov P. Analysis of strength and eigenfrequencies of a steel vertical cylindrical tank without liquid, reinforced by a plain composite thread. *Case Studies in Construction Materials*. 2023. P. 1 – 7. DOI: <https://doi.org/10.1016/j.cscm.2023.e02019>
16. Fang C., Zhang Y., Liao W., Leng X., Chen H. High-temperature corrosion behavior of structural materials in supercritical carbon dioxide. *J Mater Sci* 61. 2026. P. 51 – 75. DOI: <https://doi.org/10.1007/s10853-025-11965-5>

17. Liu B. Corrosion Behavior and Protection Technologies of Petrochemical Pipeline Materials in High-Pressure and High-Temperature Environments. *Chem Technol Fuels Oils* 61. 2025. P. 809 – 814. DOI:<https://doi.org/10.1007/s10553-025-01924-w>
18. Muthukrishnan R., Balogun Y., Rajendran V., Prathuru A., Hossain M., Faisal N.H. Machine Learning Approach to Investigate High Temperature Corrosion of Critical Infrastructure Materials. *High Temperature Corrosion of mater.* 2024. P. 309 – 331. DOI:<https://doi.org/10.1007/s11085-024-10312-4>
19. Fan R., Cao L., Hu Y., Liu X. Analysis of Corrosion Products of 316H Stainless Steel Under High Temperature on LIBS System. In: Li, X. *Proceedings of 22nd International Corrosion Congress. ICC 2024. Springer Proceedings in Materials.* 2026. P. 1 – 9. DOI:https://doi.org/10.1007/978-981-95-5196-5_3
20. Yan A., Ma J., Zhou C., Wang Y., Fan Z. Study on Automatic Characteristic Analysis and Measurement Method of High Temperature Corrosion Metallographic Image. In: Li, X. *Proceedings of 22nd International Corrosion Congress. Springer Proceedings in Materials. ICC.* 2026. P. 1 – 4. DOI:https://doi.org/10.1007/978-981-95-5196-5_26
21. Qiu L., Xiao L., Qian J. Corrosion of Alloy 800H Weldments in High – Temperature Helium Environment. *JOM.* 2026. P. 1 – 15. DOI:<https://doi.org/10.1007/s11837-025-08086-4>
22. Wang X., Xu M. Research on Anti-Corrosion and Anti – Channeling Cement Slurry System for High Temperature Well. In: Lin, J. *Proceedings of the International Field Exploration and Development Conference. IFEDC 2024. Springer Series in Geomechanics and Geoengineering.* 2025. P. 4 – 7. DOI:https://doi.org/10.1007/978-981-96-4922-8_22
23. Jena S., Swain B.P. Corrosion Properties of Coating Materials. In: Swain, B.P. *Advances in Mechanical Coating. Materials Horizons: From Nature to Nanomaterials.* 2025. P. 1 – 10. DOI:https://doi.org/10.1007/978-981-96-7484-8_10
24. Hu N., Peng W., Li J. Stress – Electrochemical Corrosion Behavior of High – Strength Steel Welded Joints in Low – Temperature Seawater Environment. In: Li, X. (eds) *Proceedings of 22nd International Corrosion Congress. ICC 2024.* P. 71. DOI:https://doi.org/10.1007/978-981-96-4894-8_22
25. Wang X., Fu K., Ren X. Effect of Laser Remelting on High-Temperature Molten Salt Corrosion Properties of Laser-Clad IN625 Coating. *J. of Materi Eng and Perform* 2025. DOI: <https://doi.org/10.1007/s11665-025-13049-6>
26. Liu Z., Liu W., Shi J., Guo X., Zhang L. Effect of Surface Condition on the General Corrosion Resistance of Several Candidate Cladding Materials. In: Tan S., Xu W., Zhu Y. *Proceedings of the 32nd International Conference on Nuclear Engineering. Weihai, China. ICONE.* 2026. P. 329. DOI:https://doi.org/10.1007/978-981-95-2732-8_53
27. Khantisopon K., Singh S., Jitputti J. Berndt C.C., Andrew S.M. High Temperature Corrosion Resistant and Anti-slagging Coatings for Boilers: A Review. *High Temperature Corrosion of mater.* 2024. P. 1 – 55. DOI:<https://doi.org/10.1007/s11085-024-10251-0>
28. Féron, D. Materials and Corrosion in Light Water Reactors. In: Shams, A., Al-Athel, K., Tiselj I., Pautz A., Kwiatkowski T. *Challenges and Recent Advancements in Nuclear Energy Systems. SCOPE.* 2026. DOI:https://doi.org/10.1007/978-3-031-64362-0_20
29. Wu Y., Yang Y., Deng J., Pan T. A study on the high-temperature air oxidation and liquid sodium corrosion behaviors of 316H steel at 700 °C. *J Mater Sci* 60. 2025. P. 6971 – 6986. DOI:<https://doi.org/10.1007/s10853-025-10855-0>
30. Alao T.O., Alao K.T., Alara O.R., Ola V.D. A Comprehensive Review of Corrosion Failure Mechanisms in Advanced Materials: Microscopic Insights and Durability Under Extreme Conditions. *High Temperature Corrosion of mater.* 2026. P. 1 – 5. DOI: <https://doi.org/10.1007/s11085-025-10358-y>
31. Kolesnikov A.S., Sergeeva I.V., Botabaev N.E., Al’zhanova A.Zh., Ashirbaev Kh.A. Chemical and phase transitions in oxidized manganese ore in the presence of carbon. *Steel in Translation.* 2017. P. 605 – 609. DOI:<https://doi.org/10.3103/S0967091217090078>

32. Sergeeva I.V., Botabaev N.E., Al'Zhanova A.Z., Ashirbaev K.A. Thermodynamic simulation of chemical and phase transformations in the system of oxidized manganese ore – carbon. *Izvestiya Ferrous Metallurgy*. 2017. 60(9). P. 759 – 765. DOI:<https://doi.org/10.17073/0368-0797-2017-9-759-765>
33. Klyuev S.V., Slobodchikova N.A., Saidumov M.S., Abumuslimov A.S., Mezhidov D.A., Khezhev T.A. Application of ash and slag waste from coal combustion in the construction of the earth bed of roads. *Construction Materials and Products*. 2024. 7 (6). P. 3. DOI: <https://doi.org/10.58224/2618-7183-2024-7-6-3>

INFORMATION ABOUT THE AUTHORS

Abshenov Kh.A., e-mail: hasen8585@mail.ru, ORCID ID: <https://orcid.org/0000-0002-0173-2524>, SCOPUS: <https://www.scopus.com/authid/detail.uri?authorId=6504208889>, M. Auezov South Kazakhstan University, Department of Mechanics and Mechanical Engineering, Shymkent, Republic of Kazakhstan, Candidate of Technical Sciences (Ph.D.), Associate Professor

Arapov B.R., e-mail: b.arapov@rambler.ru, ORCID ID: <https://orcid.org/0009-0000-0992-9797>, M. Auezov South Kazakhstan University, Department of Mechanics and Mechanical Engineering, Shymkent, Republic of Kazakhstan, Doctor of Technical Sciences (Advanced Doctor), Professor

Seitkazenova K.K., e-mail: kseitkazi@mail.ru, ORCID ID: <https://orcid.org/0000-0002-8819-7316>, SCOPUS:<https://www.scopus.com/authid/detail.uri?authorId=57151093669>, M. Auezov South Kazakhstan University, Department of Mechanics and Mechanical Engineering, Shymkent, Republic of Kazakhstan, Doctor of Technical Sciences (Advanced Doctor), Professor

Pecherskiy V.N., e-mail: vn-pecherskiy@mail.ru, ORCID ID: <https://orcid.org/0009-0002-6277-6827>, SCOPUS:<https://www.scopus.com/authid/detail.uri?authorId=59221488800>, M. Auezov South Kazakhstan University, Department of Mechanics and Mechanical Engineering, Republic of Kazakhstan, Doctor of Technical Sciences (Advanced Doctor), Professor

Zhailybek B.B., e-mail: bakdaulet.zhailybek@mail.ru, ORCID ID: <https://orcid.org/0009-0003-0483-9807>, M. Auezov South Kazakhstan University, Department of Mechanics and Mechanical Engineering, Republic of Kazakhstan, Doctoral Student

Mishra B.M., e-mail: bmishra@wpi.edu, ORCID ID: <https://orcid.org/0000-0001-7897-1817>, SCOPUS: <https://www.scopus.com/authid/detail.uri?authorId=55433568000&origin=recordpage>, Worcester Polytechnic Institute, Metal Processing Institute Director, NSF Center for Resource Recovery & Recycling, Candidate of Engineering Sciences (Ph.D.), Professor

Kedelbayev B.Sh., e-mail: kedelbaev@yandex.kz, ORCID ID: <https://orcid.org/0000-0003-0322-9743>, SCOPUS: <https://www.scopus.com/authid/detail.uri?authorId=6507190567>, M. Auezov South Kazakhstan University, Republic of Kazakhstan, Doctor of Technical Sciences (Advanced Doctor), Professor, Head of the Research Laboratories "Industrial Biotechnology"

Takibayeva G.A., e-mail: takibayevagulchekhira@gmail.com, ORCID ID: <https://orcid.org/0000-0003-2663-0281>, SCOPUS: <https://www.scopus.com/authid/detail.uri?authorId=57194064669>, M. Auezov South Kazakhstan University, Department of the Advanced Mathematics and Physics, Republic of Kazakhstan